



Probing Carrier Transport and Structure-Property Relationship of Highly Ordered Organic Semiconductors at the Two-Dimensional Limit

Yuhan Zhang,¹ Jingsi Qiao,² Si Gao,³ Fengrui Hu,⁴ Daowei He,¹ Bing Wu,¹ Ziyi Yang,¹ Bingchen Xu,¹
 Yun Li,¹ Yi Shi,^{1,*} Wei Ji,^{2,5,†} Peng Wang,³ Xiaoyong Wang,⁴ Min Xiao,^{4,6} Hangxun Xu,⁷
 Jian-Bin Xu,^{8,1,‡} and Xinran Wang^{1,§}

¹*National Laboratory of Solid State Microstructures, School of Electronic Science and Engineering, and Collaborative Innovation Center of Advanced Microstructures, Nanjing University, Nanjing 210093, China*
²*Department of Physics and Beijing Key Laboratory of Optoelectronic Functional Materials & Micro-nano Devices, Renmin University of China, Beijing 100872, China*

³*College of Engineering and Applied Sciences, Nanjing University, Nanjing 210093, China*

⁴*School of Physics, Nanjing University, Nanjing 210093, China*

⁵*Department of Physics and Astronomy, Shanghai Jiao Tong University, Shanghai 200240, China*
and Collaborative Innovation Center of Advanced Microstructures, Nanjing 210093, China

⁶*Department of Physics, University of Arkansas, Fayetteville, Arkansas 72701, USA*

⁷*CAS Key Laboratory of Soft Matter Chemistry, Department of Polymer Science and Engineering, University of Science and Technology of China, Hefei 230026, China*

⁸*Department of Electronic Engineering and Materials Science and Technology Research Center, The Chinese University of Hong Kong, Hong Kong SAR, China*

(Received 20 August 2015; published 5 January 2016)

One of the basic assumptions in organic field-effect transistors, the most fundamental device unit in organic electronics, is that charge transport occurs two dimensionally in the first few molecular layers near the dielectric interface. Although the mobility of bulk organic semiconductors has increased dramatically, direct probing of intrinsic charge transport in the two-dimensional limit has not been possible due to excessive disorders and traps in ultrathin organic thin films. Here, highly ordered single-crystalline mono- to tetralayer pentacene crystals are realized by van der Waals (vdW) epitaxy on hexagonal BN. We find that the charge transport is dominated by hopping in the first conductive layer, but transforms to bandlike in subsequent layers. Such an abrupt phase transition is attributed to strong modulation of the molecular packing by interfacial vdW interactions, as corroborated by quantitative structural characterization and density functional theory calculations. The structural modulation becomes negligible beyond the second conductive layer, leading to a mobility saturation thickness of only ~ 3 nm. Highly ordered organic ultrathin films provide a platform for new physics and device structures (such as heterostructures and quantum wells) that are not possible in conventional bulk crystals.

DOI: [10.1103/PhysRevLett.116.016602](https://doi.org/10.1103/PhysRevLett.116.016602)

Organic field-effect transistors (OFETs) offer unique advantages of low cost, light weight, and flexibility and are widely used in the electronics and display industry. While the mobility of bulk organic semiconductors has increased dramatically [1–3], an outstanding issue is to directly examine the structure-property relationship at the semiconductor-dielectric interface [4], where charge transport actually occurs [5–7]. Ultrathin organic semiconductors a few nanometers thick are often dominated by traps and disorders and far away from the intrinsic transport regime [8–10]. Another challenge in organic electronics is the development of layer-by-layer epitaxy with precision similar to molecular beam epitaxy in their inorganic counterparts [11]. These challenges may be alleviated if molecular crystals are processed into large-area, highly crystalline monolayers. Such a 2D form factor will also bring about new applications such as nanoporous membranes and insulating dielectrics [12,13]. Several recent breakthroughs in various

types of 2D organic materials such as polymers [14,15], oligomers [16], and covalent organic frameworks [17] have already shown great promise in this direction. However, one of the most fundamental questions regarding the nature of charge transport at the 2D limit has not been addressed. In this work, we study the benchmark molecule pentacene, epitaxially crystallized on a BN substrate because of its high mobility and simple structure to model. The highly clean system allows us to provide the first definitive scenario of how molecular packing and charge transport are modulated near the interface, without being dominated by extrinsic factors. Our results suggest the possibility of bandlike transport in organic materials even at the monolayer limit. This hybrid structure can also serve as a generic platform to study the intrinsic electrical and optical properties of organic semiconductors down to a monolayer.

Few-layer pentacene crystals were epitaxially grown on mechanically exfoliated hexagonal BN by the vapor

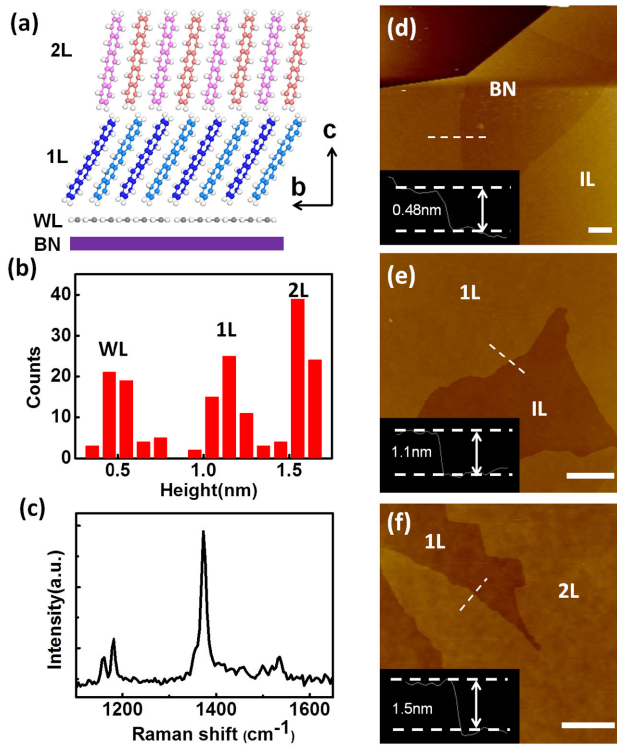


FIG. 1. Epitaxial growth of 2D pentacene crystals on BN. (a) Schematic illustration of the molecular packing of WL, 1L, and 2L within b - c plane. (b) Histogram distribution of the thickness of WL, 1L, and 2L, each taken from over 10 samples. (c) Raman spectrum of the pentacene crystals on BN, taken from a 2L sample. (d)–(f) AFM images of WL, 1L, and 2L pentacene crystals on BN, respectively. The layer numbers are marked on each image. Insets show the height profiles along the dashed lines. The scale bars are 2 μm .

transport method in a tube furnace; see Ref. [18]. The reason to choose BN as the epitaxial substrate is twofold. First, it is atomically flat with no dangling bonds and a low density of impurities, crucial to realize high-quality single-crystal pentacene films. Second, BN has a low dielectric constant, which, according to the Fröhlich polaron picture [33,34], should give a weak polaronic coupling. The growth proceeded in a layer-by-layer fashion with clear anisotropy. The frequent appearance of well-defined crystal facets [Fig. 1(f), Supplemental Material, Figs. S2b, S2c] [18] indicated that the pentacene was crystalline, as later confirmed by atomic force microscopy (AFM) and transmission electron microscopy (TEM). As schematically illustrated in Fig. 1(a), the molecular packing is very different near the dielectric interface. The average thickness of the wetting layer (WL, also referred to as interfacial layer in the literature), the first conducting layer (1L), and the second conducting layer (2L) is 0.5, 1.14, and 1.58 nm, respectively [Figs. 1(b),(d)–(f)]. The subsequent layers have the same height and molecular packing as 2L. The small thickness of WL suggests that the molecules adopt the face-on configuration (Supplemental Material, Fig. S15

[18]), similar to that of pentacene on graphite [35] and on metal [36]. The thickness of 2L is consistent with the thin-film phase of pentacene [37]. However, 1L is clearly a new polymorph, whose reduced height compared to 2L suggests more tilted molecular packing.

Further structural information of the pentacene layers was gained by high-resolution AFM. We found that both 1L and 2L were highly crystalline with the typical herringbonelike packing in the (001) plane [Fig. 2(a), Supplemental Material, Fig. S3 [18]]. The difference of lattice constants between 1L and 2L was not obvious upon initial inspection of the AFM images, but was unambiguously revealed by statistical analysis from a number of samples. As shown in Fig. 2(c), the lattice constants along the a and b axes were 6.23 ± 0.07 and 7.77 ± 0.08 Å (6.03 ± 0.05 and 7.76 ± 0.05 Å) for 1L (2L). Because of the reduced height of 1L, the unit cell expanded significantly by 0.2 Å (or 3.3%) along the a axis [Fig. 2(d)], but little expansion was observed along the b axis. More pronounced differences had also been observed along the a axis when comparing the bulk and thin-film phases of pentacene [37].

The thermal drift of AFM under ambient conditions may introduce subnanometer-scale uncertainties that cause the finite width of distributions in Fig. 2(c). Therefore, we also performed TEM characterization to crosscheck with AFM. Figure S4a in the Supplemental Material [18] shows a typical low-magnification TEM image of a few-layer pentacene on BN. Selected-area electron diffraction (SAED) was typically performed over a ~ 10 μm^2 area and exhibited a single set of diffraction patterns from pentacene [Fig. 2(b)]. Using the diffraction spots from BN as references, we determined that the lattice constants of the 2L pentacene [38] were 5.98 Å \pm 0.09 and 7.61 Å \pm 0.13 Å along the a and b axes, and the angle between them is $88.25^\circ \pm 1.22^\circ$. Together with the height measurements, we conclude that the structure of 2L is consistent with the thin-film phase of pentacene. Statistical analysis of the SAED patterns showed a sharp peak near 16° between pentacene (010) and BN (100) (Supplemental Material Fig. S4c [18]), indicating that pentacene had a quasiepitaxial relationship with BN [12]. The quasiepitaxy nature was due to weak vdW interactions and incommensurability between pentacene and BN.

Our structure measurements were further supported by *ab initio* DFT calculations [18]. Figure S17 in the Supplemental Material [18] shows the optimized molecular packing for 1L and 2L, whose lattice constants are in good agreement with experimental values within 1.5%. The packing of pentacene in each layer depends critically on the competition between intralayer and interlayer interactions: The former favors upright packing, while the latter favors face-on packing [39]. In WL, the pentacene molecules adopt a face-on configuration with the long axis along the $[11\bar{2}]$ direction of BN, because of their strong interactions of 2.35 eV/molecule (Supplemental Material, Fig. S15,

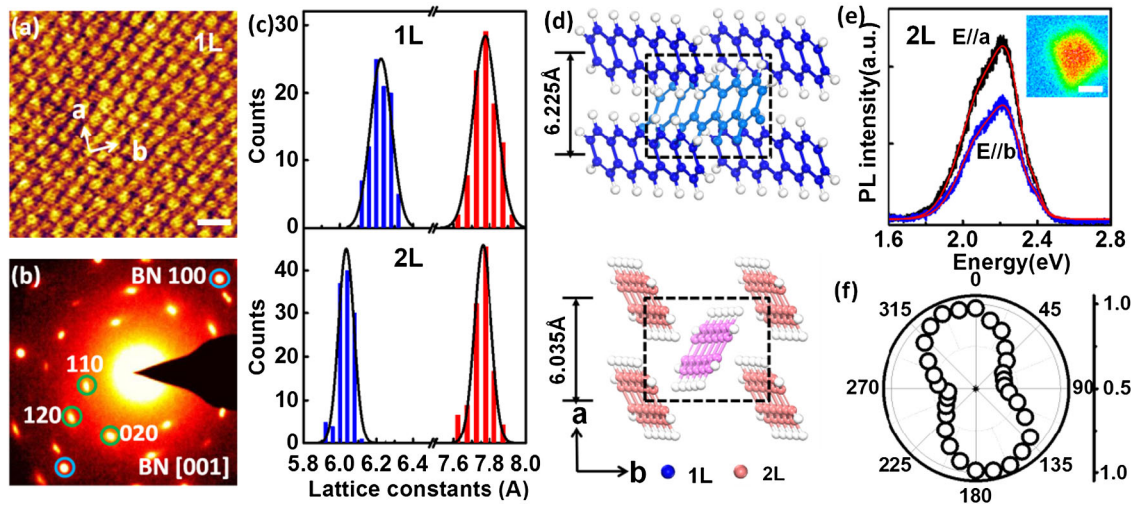


FIG. 2. Characterization of 2D pentacene crystals. (a) High-resolution AFM image of a 1L sample. The unit cell is marked. The scale bar is 1 nm. (b) SAED pattern from a few-layer pentacene sample (Supplemental Material, Fig. S4a [18] shows the low-magnification TEM image of the sample). Blue circles mark the BN (100) directions and green circles mark the pentacene (110), (120), and (020) directions. (c) Histogram of lattice constants of 1L (upper panel) and 2L (lower panel) pentacene crystals. Blue and red lines represent a - and b -axes, respectively. Black lines show the best Gaussian fittings. (d) Molecular packing of 1L (upper panel) and 2L (lower panel) pentacene within a - b plane. The unit cell is marked by the dashed rectangular box. (e) Polarization-dependent PL spectrum from a 2L sample. The black (blue) curve is taken when the PL intensity is strongest (weakest). Red lines are the fitting results with three Gaussian peaks (Supplemental Material, Fig. S6d [18]). Inset is the spatially resolved PL image of the 2L sample, showing excellent uniformity. The scale bar is 3 μm . (f) Normalized PL intensity of the 2L sample in e as a function of linear polarization angle.

Table S1 [18]). In 2L, on the other hand, the substantially reduced interlayer interaction (less than 0.3 eV/molecule) leads to the thin-film-like packing. 1L is obviously a transition between the two extremes. The leaning of molecules in 1L occurs primarily along the b axis to maximize the π - π stacking between WL and 1L. The molecules then reorient their shorter axis more parallel to the a axis, which leads to closer distance and thus more repulsion between neighboring molecules along the same direction (Supplemental Material, Fig. S17 [18]). To release this repulsion, the unit cell of 1L mainly expands along the a axis, as observed experimentally.

The pristine nature of bulk organic crystals is often manifested by the anisotropy in their optical and electrical properties [40–42]. We carried out polarization-dependent absorption and photoluminescence (PL) on 1L and 2L samples to demonstrate such anisotropy. Both absorption and PL exhibited clear and uniform modulations with a period of $\sim 180^\circ$ [Figs. 2(e), 2(f); Supplemental Material, Figs. S5, S6 [18]], presumably tailored by the crystal symmetry. The direction of the highest (lowest) PL intensity was assigned to the a axis (b axis) of the pentacene crystals [43]. Single-crystalline 1L with lateral size up to $\sim 60 \mu\text{m}$ has been observed (Supplemental Material, Fig. S5 [18]), limited by the size of BN. We note that the anisotropy of PL had only been indirectly observed in the highest quality pentacene single crystals by ellipsometry and electron energy-loss spectroscopy [43]. The PL of 1L and 2L samples composed of two prominent peaks, centered at 2.16 and 2.29 eV for 1L, and 2.13 and 2.25 eV

for 2L, as well as a small peak near 2.4 eV (Supplemental Material, Fig. S6 [18]). The splitting of ~ 0.12 eV between the two main peaks can be attributed to the Davydov splitting from the two nonequivalent molecules in a unit cell. Compared to the free exciton state in pentacene thin films and monolayers [44,45], the most striking feature was the large blue shift of exciton energy (or, equivalently, the reduction of exciton binding energy) on the order of 0.3 eV. A rough estimate gives the exciton radius of several nanometers [46], indicating their highly delocalized (or Wannier-Mott) nature likely due to the good crystallinity of the pentacene.

Next, we focus on the thickness-dependent electrical transport in pentacene crystals using backgated OFET geometry. We found that WL was not conducting within the detection limit of our instruments, consistent with the absence of intralayer π - π stacking. In the following, we focus our discussions on one representative device from 1L, 2L, and 3L, but the data were qualitatively and consistently reproduced in other devices [18]. We also checked the reversibility of our devices after thermal cycling to ensure that the observations were fully repeatable and not due to artifacts (Supplemental Material, Fig. S14 [18]).

Figure 3(a) and Supplemental Material, Fig. S7b [18] show the room-temperature transfer (I_{ds} - V_g) and output (I_{ds} - V_{ds}) characteristics of a 1L device with on-off ratio $\sim 10^8$. Several textbook features of high-quality OFET were observed in spite of the monolayer channel thickness [8]: Exceptional linearity of transfer characteristics in the linear (low bias) regime, high field-effect mobility $\mu = 1.6 \text{ cm}^2/\text{Vs}$

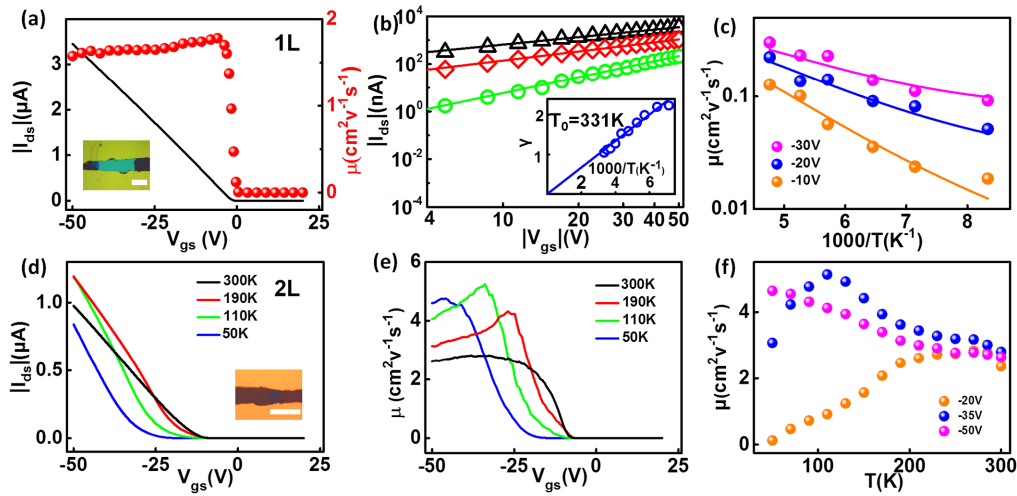


FIG. 3. Temperature-dependent electrical transport of 1L and 2L pentacene OFETs. (a) Room temperature I_{ds} - V_g characteristics ($V_{ds} = -2$ V, black line) and the extracted field-effect mobility as a function of V_g (red symbols) of a 1L device. Inset shows the optical microscope image of the device. The scale bar is $20 \mu\text{m}$. (b) I_{ds} - V_g characteristics at different temperatures of the same device under $V_{ds} = -2$ V (symbols), plotted on a double logarithmic scale. From top to bottom, $T = 300, 250$, and 140 K, respectively. The lines are power-law fitting results. Inset shows the extracted power exponent as a function of $1000/T$ (symbols). The linear fitting crosses the origin (line), consistent with the 2D hopping mechanism. $T_0 = 331$ K is derived from the linear fitting. (c) Experimental (symbols) and calculated (lines) mobility as a function of $1000/T$ under $V_g = -30$ (purple), -20 (blue), and -10 V (orange). The calculations are done with the following parameters: $T_0 = 331$ K, $\sigma_0 = 1.3 \times 10^6$ S/m, $\alpha^{-1} = 8.2$ Å. (d) I_{ds} - V_g characteristics ($V_{ds} = -2$ V) at different temperatures of a 2L device. (e) The extracted mobility as a function of V_g at the same temperatures as in (d). (f) Mobility as a function of temperature under $V_g = -20$ (orange), -35 (blue), and -50 V (purple).

(all the field-effect mobilities in this Letter are measured from the linear regime unless otherwise noted), Ohmic contact (Supplemental Material, Fig. S7c [18]), nearly zero threshold voltage ($V_{th} = 1.5$ V, corresponding to a density of deep traps $\sim 10^{11} \text{cm}^{-2}$), small subthreshold swing ($SS = 450 \text{mV/decade}$), and little hysteresis (Supplemental Material, Fig. S13a [18]).

Further insights of charge transport were inferred by temperature-dependent electrical measurements. We found that all the 1L devices exhibited insulating behavior, along with increasing nonlinearity of the I_{ds} - V_g characteristics at low temperature [Fig. 3(b)]. The transfer characteristics in the linear regime could be well described by a power-law relationship $(V_g - V_{th})^\gamma$ where the exponent adopted an inverse scaling with temperature $\gamma = (T_0/T)$. These features are signatures of 2D hopping transport [47,48]. From the linear fitting of the power exponent γ , we can extract the Urbach energy of the localized states $T_0 = 331$ K [Fig. 3(b) inset]. The Urbach energy is much smaller than disordered 2D organic semiconductors [48], and comparable to the best value for conjugated polymers [49]. By adopting the fitting procedure in Refs. [18,48], we further deduced the localization length $\alpha^{-1} \approx 0.82$ nm [Fig. 3(c)]. Another 1L device showed similar $\alpha^{-1} \approx 0.94$ nm (Supplemental Material, Fig. S9 [18]). As we shall show later with DFT calculations, the localization length ~ 1 nm is a natural result of the molecular packing in 1L.

A more surprising observation comes from 2L devices, which exhibit bandlike transport [41]. The room-temperature

field-effect mobility was typically $\sim 3 \text{cm}^2/\text{Vs}$ [Fig. 3(e)], slightly higher than the 1L devices. However, the difference in mobility became very dramatic (up to 50 times) at low temperature as the mobility of 2L devices improved as T was lowered, consistent with band transport and lack of localization [Figs. 3(d)–(f), Supplemental Material, Fig. S10c [18]]. The low-temperature field-effect mobility reached up to $5.2 \text{cm}^2/\text{Vs}$, far exceeding pentacene polycrystalline thin-film devices at similar temperatures [10,50]. The bandlike behavior could extend down to our base temperature of 50 K at high carrier density [Fig. 3(f)]. At low carrier density, the weakly insulating regime at low temperatures pointed out still finite density of shallow traps. But the large temperature and carrier density window for bandlike transport suggested rather small Urbach energy of the trap states. Indeed, Arrhenius-type fitting of the mobility in the low temperature regime gave an estimate of the Urbach energy on the order of a few meV, comparable to the thermal energy at 50 K.

The strong modulation of charge transport near the interface is unlikely from extrinsic factors such as impurities because we adopt the same material, substrate and growth procedure for 1L and 2L. To understand the molecular origin behind it, we carried out DFT calculations [18]. Figure 4 visualizes the molecular orbitals of the intermolecular bonding states for 1L (1L-B) and 2L (2L-B), which are responsible for the hole conduction in both layers (Supplemental Material, Figs. S19, S20 [18]). In 2L, the orbital overlaps horizontally, resulting in a fully extended density of states along the a and b axes that is likely

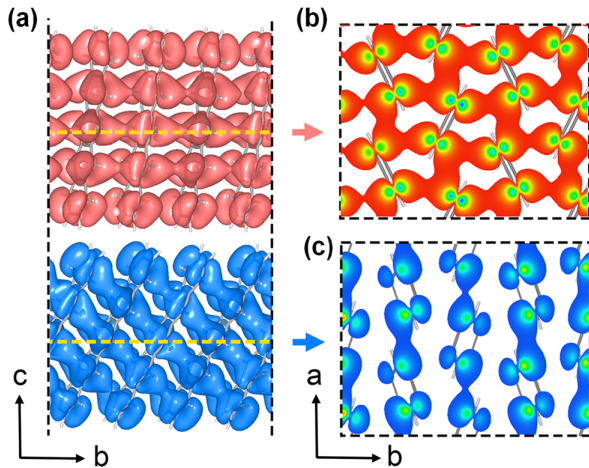


FIG. 4. Visualized molecular orbitals of the inter-molecular bonding states for 1L and 2L. (a) Side views of the molecular orbitals for 1L-B (blue) and 2L-B (red) in the b - c plane, illustrated by isosurface contours of $0.00015 e/\text{Bohr}^3$. (b)-(c) Top views of the molecular orbitals in the slices cleaved in the a - b plane for 1L-B (b) and 2L-B (c). Yellow dashed lines in (a) indicate the positions of the slices. The top phenyl group of the pentacene molecules are drawn in (b) and (c).

responsible for the bandlike transport. The more tilted molecular packing in 1L, however, substantially modifies the spatial distribution of the bonding states 1L-B, so much so that the orbitals only span for five molecules along the b axis. Therefore, a hole in 1L can only travel for ~ 1 nm before it is localized near the WL-1L interface (Supplemental Material, Fig. S20 [18]). The localization length is in excellent agreement with the experimental value without any adjustable parameters. The nature of the molecular orbitals can be more clearly visualized within the a - b plane [Figs. 4(b) and 4(c)], where 2L-B clearly forms continuous 2D networks, while 1L-B appears disconnected and localized in both directions. We believe this is mainly responsible for the distinct transport behavior in 1L and 2L. Additional reasons may include the different interlayer coupling. The transfer integral between 1L and WL has a similar magnitude to that between the adjacent 1L molecules (Supplemental Material, Table S2 [18]). This strong interlayer coupling, acting as a disorder perturbation to 1L, may cause further localization of charge carriers. The transport in 2L is nearly unperturbed from 1L, ascribed to the much smaller transfer integrals between them.

Mobility saturation is also an important issue in OFETs. Many early studies suggested that the saturation thickness was material dependent, and was ~ 6 layers (or ~ 10 nm) for polycrystalline pentacene [7]. However, the molecular understanding of the saturation thickness has remained unclear. We note that the polycrystalline thin films in those early works have high density of defects and domain boundaries, which may facilitate interlayer vertical transport. To explore this issue, we also studied 3L devices (Supplemental Material, Fig. S12 [18]). We observed the

same qualitative transport behavior as 2L devices, including room-temperature field-effect mobility $\sim 2\text{-}3 \text{ cm}^2/\text{V s}$ and bandlike transport. We thus conclude that it only takes two conducting layers (or ~ 3 nm) to reach mobility saturation in our epitaxial pentacene. This is because the modulation of molecular packing and charge transport by the substrate are already negligible beyond 2L. The small saturation thickness should be a generic attribute of high-quality layered organic semiconductors.

In conclusion, we demonstrate that vdW epitaxy of high-quality, few-layer molecular crystals can provide a powerful platform to explore their intrinsic charge transport down to a monolayer. Our results clearly show that interfacial modulation by vdW forces is an effective means to engineer the properties of organic semiconductors. We believe the highly ordered 2D molecular crystals with clean transport and excitonic properties as demonstrated here may lead to new quantum phenomena that have thus far been prevented by disorders, and to new device structures based on precise assembly of organic layers [51].

This work was supported in part by National Key Basic Research Program of China 2013CBA01604, 2015CB921600, 2012CB932704, 2015CB351900; National Natural Science Foundation of China 61325020, 61261160499, 11274154, 61521001, 11274380, 91433103, 61229401; Research Grant Council of Hong Kong SAR N_CUHK405/12; MICM Laboratory Foundation 9140C140105140C14070, a project funded by the Priority Academic Program Development of Jiangsu Higher Education Institutions, “Jiangsu Shuangchuang” program and “Jiangsu Shuangchuang Team” Program. DFT calculations were performed at the Physics Lab of High-Performance Computing of Renmin University of China and Shanghai Supercomputer Center.

Y. Z. and J. Q. contributed equally to this work.

* Corresponding authors.

yshi@nju.edu.cn

† wji@ruc.edu.cn

‡ jbxu@ee.cuhk.edu.hk

§ xrwang@nju.edu.cn

- [1] H. Li, G. Giri, J. B. H. Tok, and Z. Bao, *MRS Bull.* **38**, 34 (2013).
- [2] C. Wang, H. Dong, W. Hu, Y. Liu, and D. Zhu, *Chem. Rev.* **112**, 2208 (2012).
- [3] G. Giri, E. Verploegen, S. C. B. Mannsfeld, S. Atahan-Evrenk, D. H. Kim, S. Y. Lee, H. A. Becerril, A. Aspuru-Guzik, M. F. Toney, and Z. Bao, *Nature (London)* **480**, 504 (2011).
- [4] N. A. Minder, S. F. Lu, S. Fratini, S. Ciuchi, A. Facchetti, and A. F. Morpurgo, *Adv. Mater.* **26**, 1254 (2014).
- [5] A. Dodabalapur, L. Torsi, and H. E. Katz, *Science* **268**, 270 (1995).
- [6] F. Dinelli, M. Murgia, P. Levy, M. Cavallini, F. Biscarini, and D. M. De Leeuw, *Phys. Rev. Lett.* **92**, 116802 (2004).

- [7] R. Ruiz, A. Papadimitratos, A. C. Mayer, and G. G. Malliaras, *Adv. Mater.* **17**, 1795 (2005).
- [8] V. Podzorov, *MRS Bull.* **38**, 15 (2013).
- [9] L. Jiang, H. Dong, Q. Meng, H. Li, M. He, Z. Wei, Y. He, and W. Hu, *Adv. Mater.* **23**, 2059 (2011).
- [10] J. W. Wang and C. Jiang, *Org. Electron.* **16**, 164 (2015).
- [11] S. R. Forrest, *Chem. Rev.* **97**, 1793 (1997).
- [12] X. D. Zhuang, Y. Y. Mai, D. Q. Wu, F. Zhang, and X. L. Feng, *Adv. Mater.* **27**, 403 (2015).
- [13] H. Moon *et al.*, *Nat. Mater.* **14**, 628 (2015).
- [14] P. Kissel, D. J. Murray, W. J. Wulfstange, V. J. Catalano, and B. T. King, *Nat. Chem.* **6**, 774 (2014).
- [15] M. J. Kory, M. Worle, T. Weber, P. Payamyar, S. W. van de Poll, J. Dshemuchadse, N. Trapp, and A. D. Schluter, *Nat. Chem.* **6**, 779 (2014).
- [16] D. He *et al.*, *Nat. Commun.* **5**, 5162 (2014).
- [17] J. W. Colson, A. R. Woll, A. Mukherjee, M. P. Levendorf, E. L. Spitler, V. B. Shields, M. G. Spencer, J. Park, and W. R. Dichtel, *Science* **332**, 228 (2011).
- [18] See Supplemental Material at <http://link.aps.org/supplemental/10.1103/PhysRevLett.116.016602> for methods, supplementary figures and tables, which includes Refs. [19–32].
- [19] W. Regan, N. Alem, B. N. Alemán, B. Geng, C. a. I. Girit, L. Maserati, F. Wang, M. Crommie, and A. Zettl, *Appl. Phys. Lett.* **96**, 113102 (2010).
- [20] G. E. Pike and C. H. Seager, *Phys. Rev. B* **10**, 1421 (1974).
- [21] P. E. Blochl, *Phys. Rev. B* **50**, 17953 (1994).
- [22] G. Kresse and D. Joubert, *Phys. Rev. B* **59**, 1758 (1999).
- [23] G. Kresse and J. Furthmuller, *Phys. Rev. B* **54**, 11169 (1996).
- [24] M. Dion, H. Rydberg, E. Schroder, D. C. Langreth, and B. I. Lundqvist, *Phys. Rev. Lett.* **92**, 246401 (2004).
- [25] K. Lee, E. D. Murray, L. Z. Kong, B. I. Lundqvist, and D. C. Langreth, *Phys. Rev. B* **82**, 081101 (2010).
- [26] J. Klimes, D. R. Bowler, and A. Michaelides, *J. Phys. Condens. Matter* **22**, 074203 (2010).
- [27] J. Klimes, D. R. Bowler, and A. Michaelides, *Phys. Rev. B* **83**, 195131 (2011).
- [28] J. Heyd, G. E. Scuseria, and M. Ernzerhof, *J. Chem. Phys.* **118**, 8207 (2003).
- [29] J. Heyd, G. E. Scuseria, and M. Ernzerhof, *J. Chem. Phys.* **124**, 219906 (2006).
- [30] W. Q. Deng and W. A. Goddard, *J. Phys. Chem. B* **108**, 8614 (2004).
- [31] S. Schiefer, M. Huth, A. Dobrinevski, and B. Nickel, *J. Am. Chem. Soc.* **129**, 10316 (2007).
- [32] P. B. Paramonov, V. Coropceanu, and J. L. Bredas, *Phys. Rev. B* **78**, 041403 (2008).
- [33] I. N. Hulea, S. Fratini, H. Xie, C. L. Mulder, N. N. Iossad, G. Rastelli, S. Ciuchi, and A. F. Morpurgo, *Nat. Mater.* **5**, 982 (2006).
- [34] J. Veres, S. D. Ogier, S. W. Leeming, D. C. Cupertino, and S. M. Khaffaf, *Adv. Funct. Mater.* **13**, 199 (2003).
- [35] Y. Harada, H. Ozaki, and K. Ohno, *Phys. Rev. Lett.* **52**, 2269 (1984).
- [36] Y. L. Wang, W. Ji, D. X. Shi, S. X. Du, C. Seidel, Y. G. Ma, H. J. Gao, L. F. Chi, and H. Fuchs, *Phys. Rev. B* **69**, 075408 (2004).
- [37] S. C. B. Mannsfeld, A. Virkar, C. Reese, M. F. Toney, and Z. Bao, *Adv. Mater.* **21**, 2294 (2009).
- [38] We believe the diffractions spots mainly come from 2L and above, because the electron reflections from 1L and 1L are considerably weaker than those from the rest of the pentacene multilayers and hence not able to be recorded at the current imaging condition with a short acquisition time and low incident electron dose.
- [39] K. Kim, E. J. G. Santos, T. H. Lee, Y. Nishi, and Z. Bao, *Small* **11**, 2037 (2015).
- [40] V. C. Sundar, J. Zaumseil, V. Podzorov, E. Menard, R. L. Willett, T. Someya, and J. A. Rogers, *Science* **303**, 1644 (2004).
- [41] V. Podzorov, E. Menard, A. Borissov, V. Kiryukhin, J. A. Rogers, and M. E. Gershenson, *Phys. Rev. Lett.* **93**, 086602 (2004).
- [42] D. Y. Zang, F. F. So, and S. R. Forrest, *Appl. Phys. Lett.* **59**, 823 (1991).
- [43] M. Grobosch, R. Schuster, T. Pichler, M. Knupfer, and H. Berger, *Phys. Rev. B* **74**, 155202 (2006).
- [44] R. He, X. Chi, A. Pinczuk, D. V. Lang, and A. P. Ramirez, *Appl. Phys. Lett.* **87**, 211117 (2005).
- [45] R. He, N. G. Tassi, G. B. Blanchet, and A. Pinczuk, *Appl. Phys. Lett.* **96**, 263303 (2010).
- [46] Considering the gap between HOMO, and LUMO in pentacene is 2.2–2.3 eV [*Phys. Rev. Lett.* **93**, 086802 (2004); *Phys. Rev. B* **71**, 081202R (2005)], the observed exciton binding energy is on the order of 0.1 eV. Using a dielectric constant of 2.5 for pentacene [*Phys. Rev. Lett.* **98**, 037402 (2007)], we can estimate the exciton radius of 5.7 nm.
- [47] M. C. J. M. Vissenberg and M. Matters, *Phys. Rev. B* **57**, 12964 (1998).
- [48] J. J. Brondijk, W. S. C. Roelofs, S. G. J. Mathijssen, A. Shehu, T. Cramer, F. Biscarini, P. W. M. Blom, and D. M. de Leeuw, *Phys. Rev. Lett.* **109**, 056601 (2012).
- [49] D. Venkateshvaran *et al.*, *Nature (London)* **515**, 384 (2014).
- [50] A. R. Brown, C. P. Jarrett, D. M. deLeeuw, and M. Matters, *Synth. Met.* **88**, 37 (1997).
- [51] A. K. Geim and I. V. Grigorieva, *Nature (London)* **499**, 419 (2013).